Journal of Materials Processing Tech. 247 (2017) 158–170

Contents lists available at ScienceDirect

Journal of Materials Processing Tech.

journal homepage: www.elsevier.com/locate/jmatprotec

Determination of the interfacial heat transfer coefficient for a hot aluminium stamping process

Xiaochuan Liu[a], Kang Ji[a], Omer El Fakir[a], Haomiao Fang[b], Mohammad M. Gharbi[c], LiLiang Wang[a,*]

[a] Department of Mechanical Engineering, Imperial College London, London, SW7 2AZ, UK
[b] Nissan Motor Manufacturing, Sunderland, SR5 3NS, UK
[c] Schuler Pressen GmbH, Goeppingen, 73033, Germany

ARTICLE INFO

Keywords:
Interfacial heat transfer coefficient (IHTC)
Hot aluminum stamping
AA7075
IHTC test facility

ABSTRACT

The interfacial heat transfer coefficient (IHTC) is an important thermophysical parameter in hot stamping processes and must be identified not only to retain the full mechanical strength of formed components, but also to optimise the production rate. In this work, a novel experimental facility was developed and applied to measure the temperature evolutions of the specimens and tools in stamping processes. Simulated temperature evolutions obtained using the FE software PAM-STAMP were then fit to this data. The IHTC values between AA7075 and three different tool materials were characterized at different contact pressures under both dry and lubricated conditions. In addition, a mechanism based IHTC model was developed and validated as a function of contact pressure, tool material and lubricant thickness to predict the IHTC values under different conditions.

1. Introduction

The characteristic properties of aluminium alloys, *e.g.* high strength-weight ratio, high thermal conductance, good corrosion resistance and good recyclability, render them ideal materials to fulfil the rapidly growing demand for light-weight vehicles to reduce carbon emissions and improve fuel economies. Their low formability at room temperature, however, limits the applications of aluminium alloys in the automotive industry.

In recent years, hot stamping was developed as a promising technology to form sheet metal components at elevated temperatures. Solution Heat treatment, Forming and in-die Quenching (HFQ[1]) is one such novel sheet metal forming technology for manufacturing large complex-shaped and thin-walled components (Foster et al., 2013). The metal blank is firstly heated up to its solution heat treatment (SHT) temperature, and then formed and quenched simultaneously by cold dies at a high forming speed to obtain a supersaturated solid solution (SSSS), which provides a high post-form strength after artificial ageing (Garrett et al., 2005). In order to retain the full mechanical strength of the material during ageing processes that follow forming, the quenching rate during the hot stamping process must be above the critical cooling rate such that no solute elements precipitate out as coarse particles (Milkereit et al., 2009). The interfacial heat transfer coefficient, an important thermophysical parameter in hot stamping processes, such as HFQ, should therefore be identified not only to retain the full mechanical strength of formed components by achieving the critical quenching rates for different aluminium alloys (Liu et al., 2015), but also to optimise the production rate by controlling the quenching process. Furthermore, the critical quenching rates and the corresponding critical contact pressures are beneficial for guiding the tool design, in order to avoid insufficient quenching in particular regions, e.g. vertical walls, sharp corners, and thus providing a high post-form strength after artificial ageing.

Great efforts have been made previously to measure interfacial temperature evolutions and determine IHTC values. In Chang et al.'s (2016) hot stamping experiments, 22MnB5 specimens were heated to the target temperature of 900 °C and soaked for 3 min. The specimens were then quickly transferred onto a lower die and compressed by an upper die, which were both made of AISI 1045 tool steel, and their temperature evolutions recorded. In Bai et al.'s (2012) hot forging experiments of Ti-6Al–4 V, specimens were placed between a lower and an upper die, which were made of H13 steel. The specimens were heated by a furnace to the target temperature and then compressed between two dies heated by a band heater, while temperature histories were recorded by pairs of thermocouples. Similar compression equipment was also applied by Yukawa et al. (2014). Once heated to their

* Corresponding author.
E-mail address: liliang.wang@imperial.ac.uk (L. Wang).
[1] HFQ® is a registered trademark of Impression Technologies Ltd.

http://dx.doi.org/10.1016/j.jmatprotec.2017.04.005
Received 6 March 2017; Received in revised form 3 April 2017; Accepted 6 April 2017
Available online 08 April 2017

target temperatures and soaked for different periods of times, the specimens made of carbon steel, were moved onto a heat insulating die and compressed by a heat conducting punch. The temperature evolutions of the punch were measured and recorded using thermocouples embedded in the punch.

In order to identify the IHTC under specific experimental conditions, the measured temperature evolutions were compared with those inversely calculated with Beck's non-linear estimation method (Caron et al., 2014), or with those predicted by formulations using a 1D closed form method (Bai et al., 2012). Additionally, FE simulations (run in ABAQUS (Ji et al., 2014), PAM-STAMP (Liu et al., 2015) or DEFORM-2D (Yukawa et al., 2014)) were applied to obtain simulated temperature evolutions to fit the experimental curves to identify the corresponding IHTC values.

Several studies have also investigated factors, e.g. contact pressure, tool material and lubricant, influencing the IHTC in metal forming processes. The power increasing trend of IHTC with contact pressure was obtained by Chang et al. (2016) for hot stamping of 22MnB5 steel. The IHTC was observed to increase from 0 kW/m^{2}K at 0 MPa to around 4.5 kW/m^{2}K at 30 MPa. The result of the exponential increasing trend of IHTC with contact pressure was observed in the study by Bai et al. (2012) of Ti-6Al–4 V and Yukawa et al. (2014) of carbon steel. The effect of tool material has been characterised in Chang et al.'s (2016) study, in which 22MnB5 blanks were stamped by AISI1045 steel and H13 tool steel respectively. The thermo-physical properties e.g. the thermal conductivity and specific heat capacity, of 1045 tool steel are higher than that of H13 tool steel, contributing to higher IHTC values. Hu et al. (2013) investigated the IHTC in hot stamping between 22MnB5 blanks and H11 tools, which have thermophysical property values, and subsequently IHTC values, between those of 1045 and H13 tool steels (Chang et al., 2016). Hu et al. (1998) also found that the peak IHTC of 2.5 kW/m^{2}K between Ti-6Al–4 V and Inconel alloy IN718 at 200 MPa, was less than that of H13 (20 kW/m^{2}K) under the same conditions (Bai et al., 2012). The effect of lubricant has been investigated in Burte et al.'s (1990) study, in which graphite in water suspension was applied as a lubricant between aluminium alloy 2024-0 and H13 tool steel. The lubricant raised the IHTC values from 1.8 to 6 kW/m^{2}K at 0.85 MPa and from 9 to 18 kW/m^{2}K at 150 MPa. This positive effect of lubricant on the IHTC was also observed in the study by Foster et al. (2008) of AA6082 using four different lubricants and by Jain, (1990) for Al1100-O using MoS_2 as a lubricant. However, the reverse effect was found in Zhang et al.'s (2010) research, in which glass was used as a lubricant.

The IHTC therefore depends on the contact pressure, the material of the contact bodies and the lubricant. In order to predict its value, Çetinkale and Fishenden, (1951)'s equation is widely used to estimate the general heat transfer coefficient, as shown in Eq. (1).

$$h = h_g + h_c \tag{1}$$

where h_g and h_c are the heat transfer coefficients across the air gap and for the solid contact respectively.

Cooper and Yovanovich, (1969) identified a theoretical model for the IHTC between two contact solid bodies, as a power function of contact pressure, as shown in Eq. (2):

$$h = 1.45k\frac{\tan\theta}{\sigma}\left(\frac{p}{H}\right)^{0.985} \tag{2}$$

where k is the mean thermal conductivity of two contact bodies, θ is the mean of the absolute slope of the surface profile and σ is the standard deviation of the profile heights.

As shown in Eq. (3), a power relationship between the IHTC and contact pressure was also developed as an empirical model by Shlykov et al. (1977):

$$h = 8000\overline{\lambda}\left(\frac{p}{C\sigma_U}K\right)^{0.86} \tag{3}$$

where $\overline{\lambda}$ is the mean thermal conductivity of the two contact bodies, σ_U is the ultimate strength of the test specimens, and K and C are model coefficients.

Differing from the models above, an exponential equation for IHTC as a function of contact pressure was developed by Yukawa et al. (2014), as shown in Eq. (4):

$$h = A(1 - \exp(-BP)) \tag{4}$$

where A and B are model constants determined by the least square method using the experimental results.

In order to characterise the IHTC values under a lubricated condition, an equation was built up by Wilson et al. (2004), as shown in Eq. (5):

$$h = \frac{1-A}{h_f}\frac{2k_fk_tk_w}{2k_tk_w - k_wk_f - k_fk_t} \tag{5}$$

where A is the contact area, h_f is the applied lubricant thickness, and k_f, k_t and k_w are the thermal conductivities of the lubricant, tool and workpiece, respectively.

In the present research, a novel experimental facility was developed and applied to measure temperature evolutions of specimens and tools at different contact pressures under dry and lubricated conditions. The facility, designed with interchangeable components, streamlines the process by which the IHTC between different combinations of blank and tool materials could be determined. The IHTC value was subsequently found by utilising an inverse technique to fit the experimental data to simulated temperature evolutions obtained using the FE software PAM-STAMP. The capabilities of the IHTC test facility are demonstrated here by using it to investigate the effect of contact pressure and lubricant on the IHTC between a hot AA7075 specimen and three different tools. In addition, an IHTC model was developed as a function of contact pressure, tool material and lubricant to predict their effect on the IHTC, and validated using the results of hot stamping tests of a hemispherical dome shape and B pillar component.

2. Methodology

2.1. Design of the IHTC test facility

The IHTC test facility, a schematic for which is shown in Fig. 1, was developed to simulate hot stamping processes. Three sets of punches and dies were available, made from three different tool steels, i.e. H13, cast iron and P20, with contact surfaces of 50 × 25 mm^2. The average surface roughnesses of H13, cast iron and P20 tools were 980, 810 and 960 nm respectively, and were measured using White Light Interferometry equipment (Wyko NT9100). A specimen (No. 1 in Fig. 1) was screwed onto two blankholders (No. 4 in Fig. 1), and heated using direct resistance heating, then compressed against a fixed die (No. 3 in Fig. 1) by a moving punch (No. 2 in Fig. 1).

During these temperature/pressure-sensitive IHTC tests, the compressive loads were only able to reach the target value in 0.3 s after compression was initiated, with an approximate 20 °C temperature loss in the samples; this was accounted for when comparing with the simulation results. Variable heating and cooling can be realised in both the test facility and in the simulations to represent particular processes, e.g. multi-paint cycles. Variable loads and stamping speeds can be controlled accurately, which can also be assigned in simulations to simulate different forming processes, e.g. warm/hot stamping.

The IHTC test facility provides a high stability and repeatability in the test results. Specifically, the specimens were controlled precisely to be compressed at the centre of the tools in each test with a tolerance of 0.1 mm, thus ensuring that the heat transfer between the specimen and

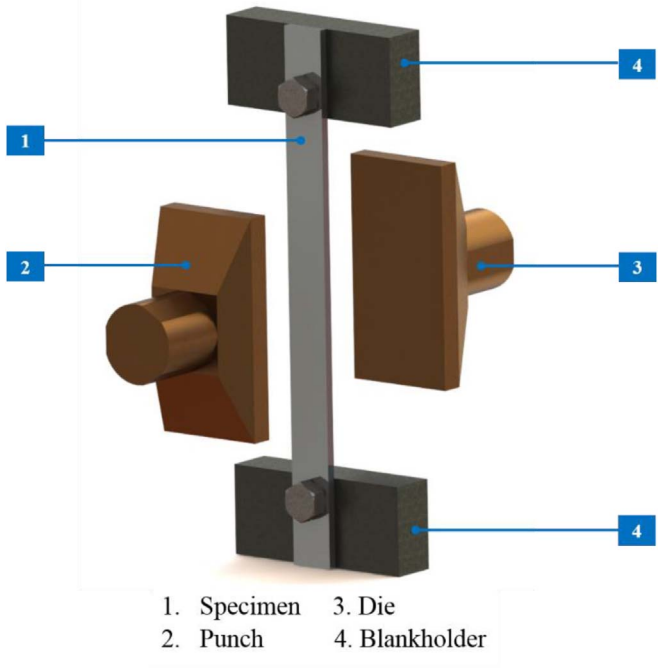

Fig. 1. Overall schematic structure of the IHTC test facility.

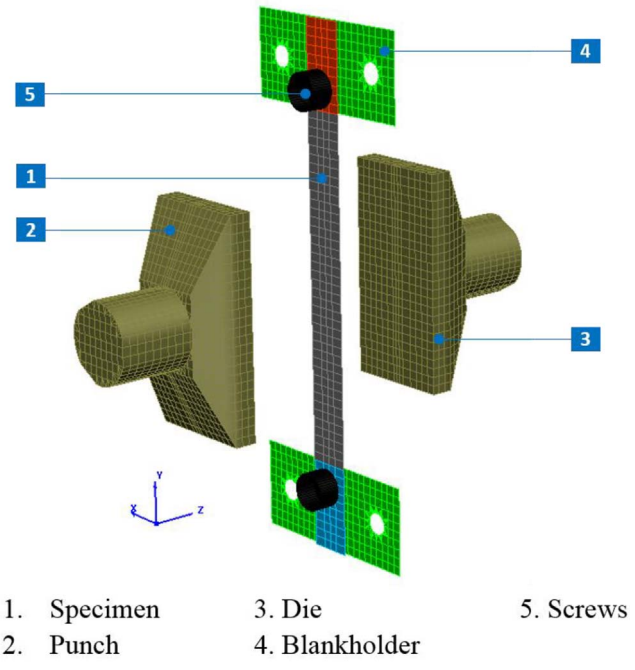

Fig. 2. The FE model of the IHTC test facility in PAM-STAMP.

tools was in three dimensions and symmetric. Additionally, the specimens were heated by direct resistance heating from their respective tops and bottoms simultaneously, ensuring a high temperature homogeneity in the compression region. The measured temperature difference between the centre and edges of the compression regions in the specimens was within 5 °C. After heating, the IHTC test facility also does not necessitate the transfer of the specimens from a furnace to a press machine. Therefore, the punch, which only takes 0.05 s to compress the specimens at a speed of 400 mm/s, could be actuated immediately after heating, ensuring a negligible temperature loss from the specimens. The initial temperature of both the punch and die could also be considered as being equivalent when the compression process was started.

2.2. Experimental procedures

Prior to each test, a 120 × 10 × 2 mm^3 AA7075 specimen supplied by AMAG Austria Metal AG in the T6 condition, was screwed onto the blankholders and positioned between the punch and die. The average surface roughness of the specimens was 340 nm and the composition of AA7075-T6 is shown in Table 1. In order to monitor temperature, pairs of thermocouples were embedded mid-thickness at the centre of the specimen, and at a distance of 3 mm below the centre of the tool (punch and die) contact surfaces respectively, and then connected to a data logger.

To represent a hot stamping process, the specimen was firstly heated by direct electrical resistance heating to its SHT temperature, 490 °C, at a heating rate of 10 °C/s, while the temperature of the tools was maintained at room temperature. Once the target temperature was reached, the punch was instantly actuated to move towards the specimen at a speed of 400 mm/s and compress it against the die at different pre-defined contact pressures. After the compression, the punch was moved back to its initial position. The temperature evolutions of the specimen and the tools were recorded throughout the compression process. Prior to each test for the lubricated condition studies, grease-based graphite was applied with great care onto the tool surfaces only, which were thoroughly cleaned by using a chemical etchant after each test. The applied layer thickness of lubricant was precisely measured by using dedicated equipment.

2.3. FE simulation procedures

In order to simulate temperature evolutions of the specimen and tools, a FE model was built up in PAM-STAMP, which enables modelling of the interactions between mechanical and thermal fields (Karbasian and Tekkaya, 2010) and that can model heat transfer in 3D. The dimensions of the specimen and tools were the same as those used in the IHTC test facility, as shown in Fig. 2. The material properties of the specimen were generated by using empirical fittings as a function of temperature in Kelvin (Johnson, 2004), and the material properties of the three tools were based on a professional online material information resource (MatWeb, 2016), and are shown in Table 2.

Explicit quadrangle thermal shell elements with two degrees of freedom in temperature were used for the specimen to precisely represent the heat transfer mechanism that occurs during the hot stamping process. The selected element size, 2 mm, ensured that the temperature at the centre of the specimen could be captured accurately while providing a reasonable computational time. The same element type and size were selected for the majority of the regions on the tools, whilst explicit triangle thermal shell elements were used for some regions near circular edges. The total number of elements of the specimen (No.1 in Fig. 2), punch/die (No.2 & 3 in Fig. 2), blankholders (No.4 in Fig. 2) and screws (No.5 in Fig. 2) were 240, 325, 634 and 216 respectively.

'Hotforming double action validation' was selected as the simulation

Table 1
The chemical composition of AA7075.

Element	Si	Fe	Cu	Mn	Mg	Cr	Zn	Ti	Ti + Zr	Others Each	Al
Wt%	0.09	0.13	1.4	0.05	2.6	0.19	5.7	0.03	0.04	0.02	Bal.

Table 2
Material properties of the specimen and tools.

Property	AA7075
Young's modulus (MPa)	$-39.082T + 82532$
Density (kg/m^3)	$-6.7537e\text{-}05T^2 - 0.15T + 2.8608e03$
Thermal conductivity (kW/mK)	$-5.145e\text{-}08T^2 + 1.368e\text{-}04T + 0.085224$
Specific heat capacity (J/kgK)	$8.721e\text{-}07T^3 - 1.4625e\text{-}03T^2 + 1.2T + 608.3$
Poisson's ratio (−)	$3.893e\text{-}08T^2 + 0.000013505T + 0.325165$
Thermal expansion (−)	$0.0216T + 16.499$

Property	H13	Cast iron	P20
Young's modulus (GPa)	210	101.4	205
Density (kg/m^3)	7.8e03	7.15e03	7.85e03
Thermal conductivity (kW/mK)	0.0244	0.044	0.0315
Specific heat capacity (J/kgK)	460	465	473
Poisson's ratio (−)	0.3	0.29	0.285

process type in PAM-STAMP, and was composted of four individual stages; gravity, holding, stamping and quenching. All six degrees of freedom were restricted for the die, whilst all degrees of freedom, except for that in the z-direction (direction of punch motion), were restricted for the punch, blankholders and screws. The specimen was able to deform in all degrees of freedom. In the gravity and holding stages, the specimen was located and held by the blankholders and screws. In the subsequent stamping and quenching stages, the punch moved towards the specimen at the same speed as that in the experiments and compressed it against the die for 4 s.

Prior to the quenching stage, the actual measured temperature from the experiments at the two ends of the specimen was 310 °C, due to the heat transfer to the blankholders, whilst the temperature distribution within the compression region was uniform. Therefore, the initial temperature of the tools, the two ends of the specimen and the centre of the specimen were set as 25, 310 and 490 °C respectively. Differing from the experiments, a different constant IHTC value was assigned for each simulation to eliminate the effect of contact pressure on the temperature evolution. The temperature evolutions, at identical locations to those in the experiments, were then plotted and compared with the experimental temperature evolutions. The experimental and simulated curves with the best agreement indicated that the IHTC assigned in that simulation was the corresponding value at the selected experimental conditions.

Fig. 3 shows a comparison of the temperature evolutions obtained from a simulation assigned an IHTC value of 9.2 kW/m^{2}K and from an experiment with a contact pressure of 3 MPa under dry conditions, using cast iron tools. From the results, it was found that the temperature of the specimen dropped drastically in the first 2s, while the punch temperature increased gradually with time. The experimental temperature evolutions agree well with the simulated curves, which indicates that the IHTC value is 9.2 kW/m^{2}K when the contact pressure is 3 MPa under dry conditions, using cast iron tools.

3. Results and discussion

3.1. Effect of contact pressure on IHTC

As shown in Fig. 4, when H13 was used as the tool material, the IHTC increases considerably from 0.7 kW/m^{2}K to approximately 8.2 kW/m^{2}K when the contact pressure increases from 0 to 7 MPa under dry conditions, followed by a gentle increase as the contact pressure increases from 7 to 10 MPa. When the contact pressure is higher than 13 MPa, a plateau of the IHTC is observed, with value of approximately 8.6 kW/m^{2}K. The variation of the IHTC values can be explained by the evolutions of real contact area at different contact pressures. The real contact area between the specimen and tools is usually much less than the apparent contact area, and increases with increasing contact pressure due to the variation of the specimen surface condition (Buchner et al., 2009). This is beneficial for the interfacial heat transfer between the specimen and the tools, leading to an increase in the IHTC with increasing contact pressure.

In order to characterise the relationship between the real contact area and contact pressure, the average surface roughness of the H13 tools and the specimens were measured after the IHTC tests. The average surface roughness of the H13 tools remained stable at 980 nm throughout the experiments, whilst for the specimen this value varied with the contact pressure. The strength of H13 within the temperature range used in the experiments was much larger than that of AA7075 at elevated temperatures. As a result, the surfaces of the specimens were deformed by the tools during the hot stamping processes and thus the surface roughness of the specimens increased correspondingly. Therefore, the real contact area was growing due to the fact that the two contact surfaces were increasingly meshed together. As shown in

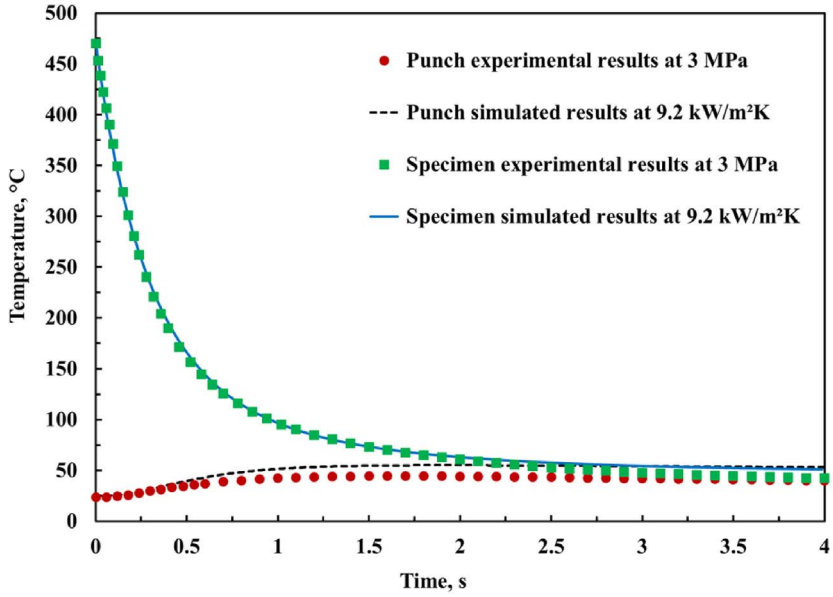

Fig. 3. The comparison between experimental and simulated temperature evolutions at a contact pressure of 3 MPa under dry conditions, using cast iron tools.

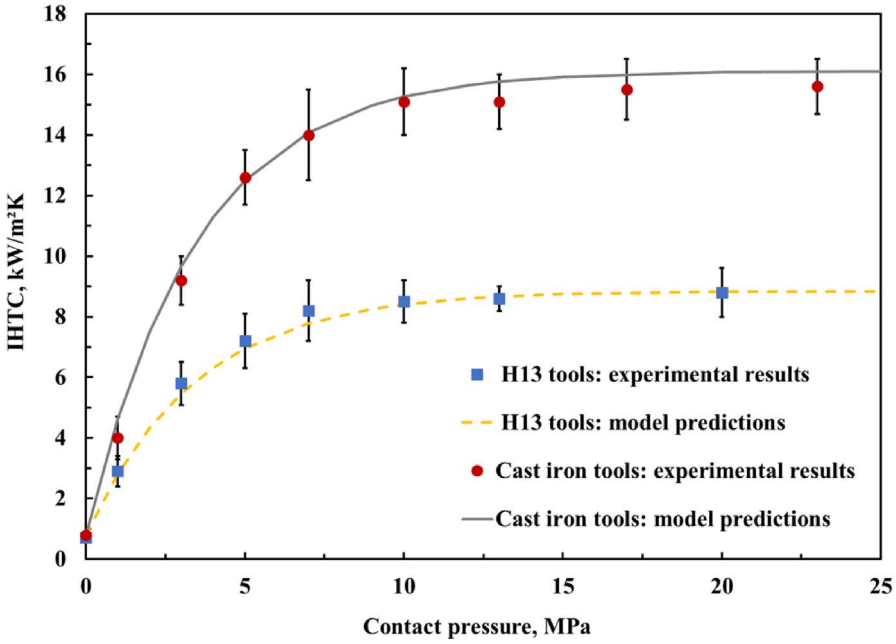

Fig. 4. The IHTC evolutions with contact pressure using H13 and cast iron tools under dry conditions.

Fig. 5, the surface roughness of the specimen increases slightly from 340 to 380 nm as the contact pressure increases from 0 to 5 MPa. During this stage, deformations occur at the surface of the specimen and thereby the real contact area increases. After the experiments, the elastic deformations recover but the plastic deformations remain. As a result, the surface roughness of the specimen increases slightly, but results in a rapid growth of the IHTC value. After yielding, the surface roughness increases dramatically from 380 nm at 5 MPa to 860 nm at 10 MPa, and correspondingly the IHTC value continues to grow rapidly. When the pressure is larger than 10 MPa, the surface roughness of the specimen increases gently to 910 nm, approaching the value for that of the H13 tools. During this stage, the two contact surfaces are meshed to the maximum extent and thus the real contact area reaches its peak. Consequently, a plateau of the IHTC is observed.

In general, the critical quenching rate for AA7XXX alloys is above 50 °C/s and this value is alloying element dependent, i.e. a higher critical quenching rate is required for an increasing content of alloying elements. Through superimposing the quenching curves obtained from the experimental temperature evolutions with the continuous cooling transformation (CCT) diagrams for the present aluminium alloy, the required contact pressure to achieve the critical cooling rate could therefore be identified. An excessive contact pressure could also be prevented from being applied between the two contact surfaces by accounting for the plateau value of the IHTC. This would be beneficial to the reduction of tool wear, the extension of tool service life and the promotion of cost efficiency in hot stamping processes.

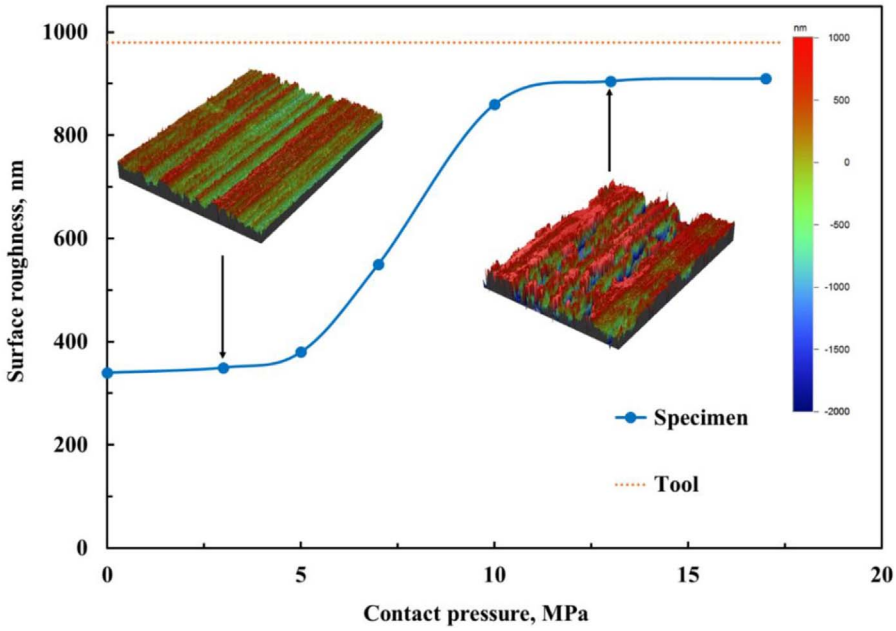

Fig. 5. The surface roughness evolution of the specimen with contact pressure after IHTC tests using H13 tools.

3.2. Effect of tool material on IHTC

When cast iron tools were applied, the overall evolution of the IHTC under dry conditions followed a similar trend to that of H13 tools, i.e. a sharp increase at the initial stage, followed by a plateau at high contact pressures, as shown in Fig. 4. Specifically, the IHTC increases dramatically from 0.8 kW/m^{2}K at 0 MPa to 14 kW/m^{2}K at 7 MPa. When the contact pressure reaches 13 MPa, the IHTC converges to a value of 15.1 kW/m^{2}K. The application of cast iron tools increases the peak IHTC value by approximately 76%, compared to when H13 tools were used. Within the temperature range used in the experiments, the average thermal conductivity of cast iron, 0.044 kW/mK, is approximately 80% higher than that of H13, which is 0.0244 kW/mK, as shown in Table 1. This indicates that the heat transfer occurs at a higher rate across cast iron tools than across H13 tools, thus leading to the greater IHTC values. The difference in the specific heat capacity between H13 (460 J/kgK) and cast iron (465 J/kgK) is negligible in this study. It would therefore be desirable to deduce the influence of the thermal conductivity of the different tools on their resulting different IHTC values. This influence could be verified by the study of Liu et al. (2015) in which the peak IHTC value for AA7075 under dry conditions when using mild steel tools, 12.3 kW/m^{2}K, lies between the peak values obtained when using H13 and cast iron tools, and the thermal conductivity of mild steel is in between both H13 and cast iron.

The temperature distributions in specimens and tools, either uniform or tailored, play a very important role in hot stamping processes, influencing the post-form strength and thickness distribution of the formed component. The application of different contact pressures and different materials in specific regions of tools are notable and influential factors that could achieve desired temperature distributions. Tool materials with a high thermal conductivity, e.g. cast iron, can be used for the punch and die for manufacturing quenching rate sensitive materials. Meanwhile, materials with a low thermal conductivity, e.g. H13, can be used for blankholders to prevent the temperature of a specimen from dropping significantly in the blankholding regions of a forming tool during forming, thus enabling more material to be drawn into the tool cavity.

Compared with previous research, the IHTC values of AA7075, using either H13 or cast iron tools, are much higher than those of Ti-6Al–4 V, 22MnB5 steel and carbon steel, thus resulting in much shorter required quenching times for hot stamping processes. In addition, the contact pressure values at which the IHTC value plateaus, using either H13 or cast iron tools, are much lower than those of titanium alloys and high strength steels, due to the lower strength of aluminium alloys at elevated temperatures. This desirable feature would reduce the requirements of the capabilities of the forming press, and extend the tool life.

3.3. Effect of lubricant on IHTC

When a grease-based graphite lubricant was applied onto the surfaces of cast iron tools, the overall evolution of the IHTC followed an exponentially increasing trend. As shown in Fig. 6, when the applied lubricant layer thickness is 0.015 mm, the IHTC increases dramatically from 3 kW/m^{2}K at 0 MPa to 19 kW/m^{2}K at 7 MPa. When the contact pressure reaches 13 MPa, the IHTC converges to a value of 22 kW/m^{2}K. The application of lubricant increases the peak IHTC values by approximately 46%, compared to that under dry conditions, using cast iron tools. The thermal conductivity of the grease-based graphite lubricant is 0.024 kW/mK, which is much higher than that of air, thus the heat flow is much more rapid when the lubricant fills up the vacancies of the asperities at the contact interface. In addition, the graphite lubricant is able to dissipate more heat to accelerate the heat transfer.

The evolutions of the IHTC are also determined as a function of the applied lubricant layer thickness at different contact pressures, as shown in Fig. 7. When the contact pressure is 5 MPa, the IHTC increases dramatically from 12.6 to 16.5 kW/mK when the applied lubricant layer thickness increases from 0 to 0.015 mm. The IHTC then remains stable when the thickness is larger than 0.015 mm. The same trend can be observed at a contact pressure of 10 MPa, i.e. as the applied lubricant layer thickness increases, a steep increase followed by a plateau of the IHTC values is observed. The IHTC value is larger when more lubricant fills up the vacancies at the contact interface. However, the excessive lubricant is squeezed out of the contact area by the tools when the lubricant thickness is greater than 0.015 mm at both contact pressures of 5 and 10 MPa, indicating that this value is the maximum effective applied lubricant layer thickness.

Contrary to the previous research (Zhang et al., 2010) conducted using glass as a lubricant, the application of grease-based graphite lubricant has a positive influence on the IHTC. It is due to the fact that the thermal conductivity of the grease-based graphite lubricant (0.024 kW/mK) is much larger than that of the glass lubricant (0.00125 kW/mK). Consequently, the heat transfer between the contact solids is much more rapid and the heat loss is significantly less when

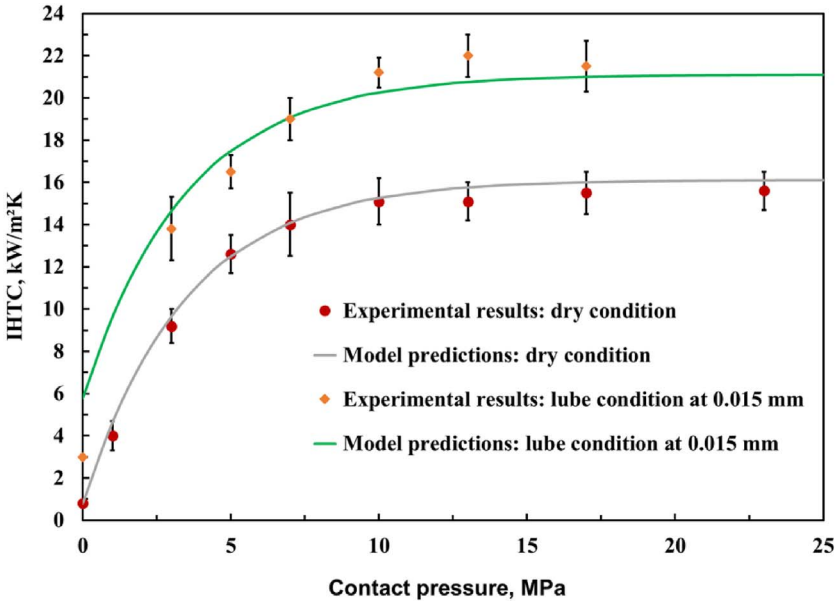

Fig. 6. The IHTC evolutions with contact pressure using cast iron tools under dry and lubricated conditions.

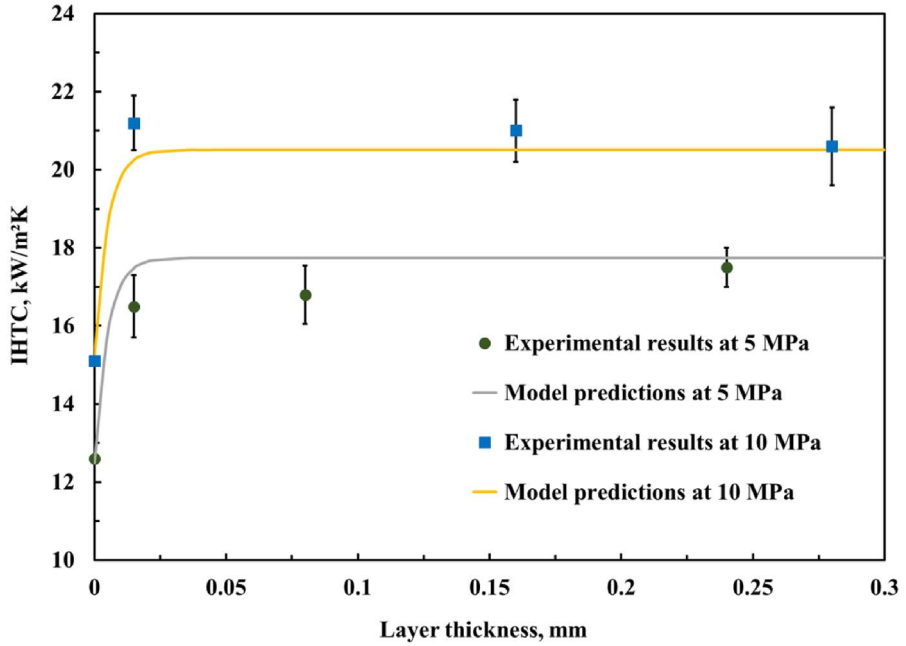

Fig. 7. The IHTC evolutions with applied lubricant layer thickness using cast iron tools, at contact pressures of 5 and 10 MPa.

using the graphite lubricant. Therefore, the application of a lubricant with a higher thermal conductivity would result in higher IHTC values and thus a shorter required quenching time for hot stamping processes. The critical contact pressure and friction would thereby be reduced, extending the tool life. Excessive lubricant could also be prevented from being applied. Overall, these features would be beneficial to the promotion of cost efficiency in hot stamping processes.

4. Development of a mechanism based IHTC model

The results obtained using the IHTC test facility at different contact pressures and for different tool materials under both dry and lubricated conditions were used to develop a definition of the overall IHTC between the specimen and tools, derived from the null-pressure IHTC h_a, solid-contact IHTC h_c and lubricant-contact IHTC h_l, as shown in Eq. (6).

$$h = h_a + h_c + h_l \tag{6}$$

where h_a represents the heat transfer across the air gap between the specimen and tools with zero pressure, and typically has a low value, h_c represents the contact under pressure between two solid surfaces, and h_l represents the application of lubricant between two solid surfaces. Eq. (6) is developed based on Çetinkale and Fishenden's, (1951) equation, which is widely used as a general model to estimate the general heat transfer coefficient. It was found that the null-pressure IHTC h_a did not play an important role in the present research since the initial amount of heat transfer between the contact surfaces was negligible according to the experimental observations. Once a contact pressure was applied, the heat transfer between the contact surfaces was increased significantly under both dry and lubricated conditions, thus the overall IHTC was mainly characterised by the solid-contact IHTC h_c and the lubricant-contact IHTC h_l. Therefore, it was reasonable to assume a constant value for the null-pressure IHTC h_a of approximately 0.8 kW/m^{2}K, which was determined by running IHTC tests under dry conditions with zero contact pressure. The solid-contact IHTC h_c, induced by the applied contact pressure, was modelled by Eq. (7):

$$h_c = \alpha \frac{K_{st} N_P}{R} \tag{7}$$

where α is a model parameter, K_{st} is the harmonic mean thermal conductivity of the contact solids, R is the root mean square of surface roughness of the contact solids and N_P is a pressure dependent parameter. The solid-contact IHTC h_c depends on the thermal conductivity of the two contact solids and the contact surfaces. Eq. (7) therefore was developed combining the physical mechanism of the heat transfer between the contact surfaces and the theory of Cooper and Yovanovich, (1969). The amount of heat transfer was considered to increase with the increasing thermal conductivity of both the specimen and tools. The solid-contact IHTC h_c is thus correlated positively with the harmonic mean thermal conductivity K_{st}. In order to simplify the model, the harmonic mean thermal conductivity K_{st} shown in Eq. (8) was determined from the average thermal conductivities of the specimen k_s and tools k_t, in the temperature range used in the experiments:

$$K_{st} = \frac{2}{k_s^{-1} + k_t^{-1}} \tag{8}$$

Meanwhile, the amount of heat transfer reduced with the decreasing real contact area between the specimen and tools, which was associated with a higher initial surface roughness of the contact surfaces. Hence a negative relationship between the solid-contact IHTC h_c and the root mean square (r.m.s.) of the initial surface roughness of the specimen and tools R was considered. The r.m.s. surface roughness was determined by the average surface roughness of the specimen R_s and tools R_t, as shown in Eq. (9):

$$R = \sqrt{R_s^2 + R_t^2} \tag{9}$$

The heat transfer was more rapid when the contact pressure increased, as the real contact area between the contact surfaces was increased. Hence this results in a positive correlation between the solid-contact IHTC h_c and the pressure dependent parameter N_P, which can be represented by the following exponential-law equation, Eq. (10):

$$N_P = 1 - \exp\left(- \lambda \frac{P}{\sigma_U} \right) \tag{10}$$

where λ is a model parameter, P is the contact pressure between the specimen and tools, and σ_U is the ultimate strength of AA7075 at 490 °C. In order to increase the IHTC values, a contact pressure could be applied, deforming the asperities on the specimen surface and thus enlarging the real contact area between the specimen and tools. The

Table 3
Material constants and model parameters of IHTC model.

k_s (kW/mK)	k_t (H13)	k_t (Cast iron)	k_t (P20)	k_l (Lubricant)
0.14	0.0244	0.044	0.0315	0.024

R_s (m)	R_t (H13)	R_t (Cast iron)	R_t (P20)	h_a (kW/m^{2}K)
3.4e-7	9.8e-7	8.1e-7	9.6e-7	0.8

σ_U (MPa)	α (−)	λ (−)	β (−)	γ (m^{-1})
21	2.01e-4	6.05	1.1e-4	2e5

ratio of the applied contact pressure to the ultimate strength (Cooper et al., 1969) (hardness (Shlykov et al., 1977)) of a specimen is equal to the ratio of the real contact area to the apparent contact area. Eq. (10) therefore represents the deformation mechanism of the asperities on the specimen surface.

When the lubricant was applied, the lubricant-contact IHTC h_l also contributed to the overall IHTC value, which was modelled by Eq. (11):

$$h_l = \beta \frac{K_{stl} N_L}{R} \tag{11}$$

where β is a model parameter, K_{stl} is the harmonic mean thermal conductivity of the three contacting materials, i.e. the tools, lubricant and specimen, R is the root mean square of the surface roughness of the two contact solids and N_L is a layer thickness dependent parameter. When a lubricant layer was introduced between the two contact solids, the heat flowed through these three contacting materials; hence the harmonic mean thermal conductivity K_{stl} is correlated positively with h_l. The harmonic mean thermal conductivity was calculated as shown in Eq. (12).

$$K_{stl} = \frac{3}{k_s^{-1} + k_t^{-1} + k_l^{-1}} \tag{12}$$

where k_s, k_t and k_l are the average thermal conductivities of the specimen, tools and grease-based graphite lubricant respectively.

The applied lubricant layer thickness is an influential factor on the lubricant-contact IHTC h_l, which can be represented by the following exponential-law equation, Eq. (13):

$$N_L = 1 - \exp(-\gamma\delta) \tag{13}$$

where γ is a model parameter and δ is the applied lubricant layer thickness.

The IHTC model was calibrated using the experimental data from the tests carried out under dry and lubricated conditions using two different tool materials. Table 3 lists the identified material constants and certain model parameters.

In order to verify the predicted results generated by the IHTC model, the material constants for P20 were used to predict the evolution of the IHTC with contact pressure under both dry and lubricated (0.015 mm layer thickness) conditions, assuming that P20 was used as the tool material, as shown in Fig. 8. These IHTC evolutions, rather than constant values, were then implemented in the FE simulation to simulate temperature evolutions using P20 tools with a contact pressure of 3 MPa under dry conditions, and 13 MPa under lubricated conditions with a layer thickness value of 0.015 mm. Meanwhile, two new tests were conducted under the same conditions as those of the simulations using the IHTC test facility. As shown in Fig. 9, it is evident that the simulated temperature evolutions were in close agreement with the experimental curves, indicating that when using P20 tools, the IHTC values at 3 MPa under dry conditions and at 13 MPa under lubricated conditions with a layer thickness value of 0.015 mm, are 6.7 and 14.5 kW/m^{2}K respectively.

Therefore, the IHTC model developed in the present research enables the prediction of IHTC evolutions as a function of contact pressure, tool material and lubrication. When using certain materials

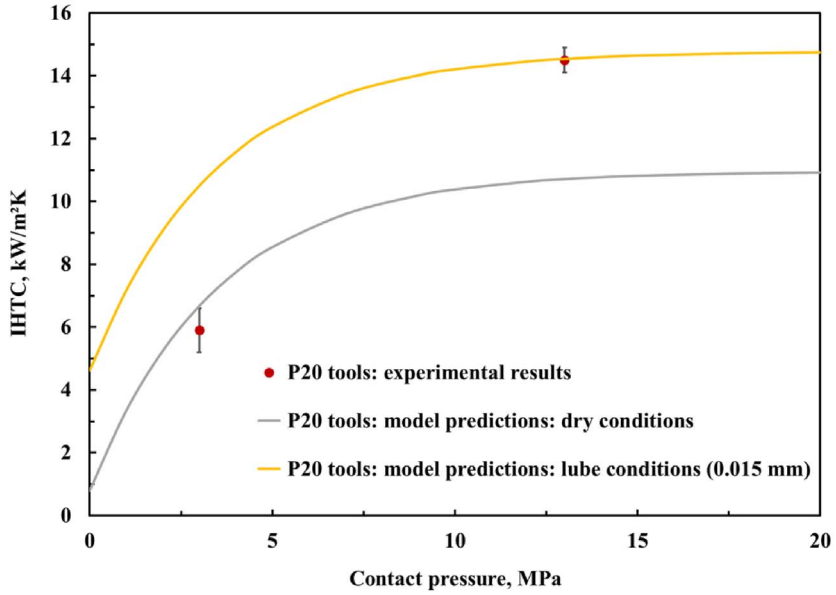

Fig. 8. The predicted IHTC evolutions with contact pressure using P20 tools under dry and lubricated conditions.

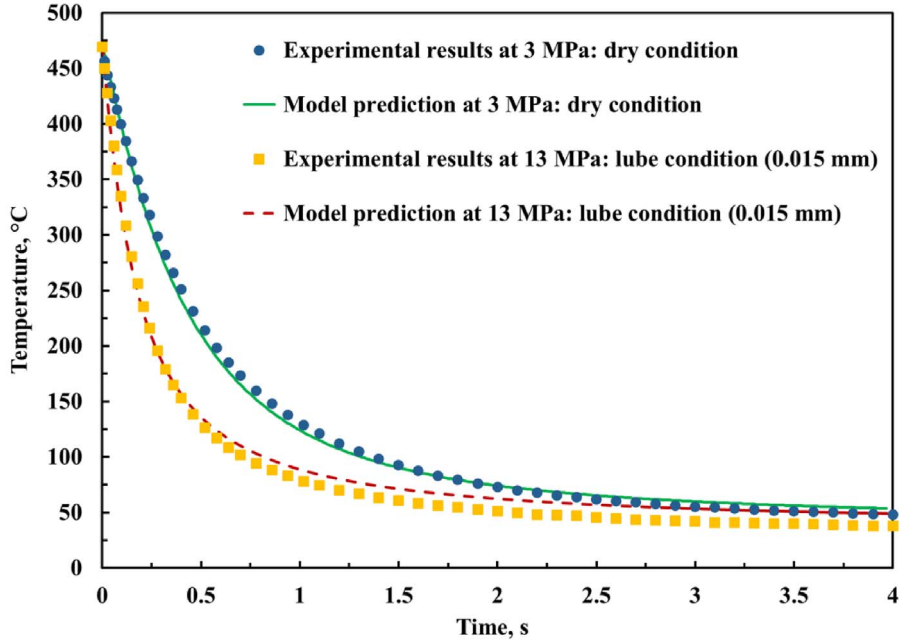

Fig. 9. The experimental and model predicted temperature evolutions at 3 MPa under dry conditions and 13 MPa under lubricated conditions, using P20 tools.

for the specimens, tools and lubricant, the IHTC evolution comprises two stages; a rapidly increasing stage due to the introduction of the contact pressure, and a stable stage due to the achievement of the convergent contact pressure value at which the IHTC becomes constant.

If specimens and tools with higher thermal conductivity values are used, the corresponding IHTC evolutions will have higher values due to a greater amount of heat transfer between the two contact solids. Fig. 10 shows IHTC evolutions as a function of the thermal conductivity of the tool and specimen, predicted by the IHTC model, at a constant contact pressure of 15 MPa and surface roughness of 810 and 340 nm for the tool and specimen respectively, under dry and lubricated (0.02 mm layer thickness) conditions. The IHTC values for AA7075 using tools with a greater thermal conductivity than that of cast iron tools, e.g. AISI 1045 tool steel, will therefore be higher. When using cast iron tools, the IHTC values for some aluminium alloys with a smaller thermal conductivity than that of AA7075, e.g. AA5083, will thus be lower under the same conditions. In addition, the application of lubricant enhances the IHTC values, indicating that using tools with a lower thermal conductivity, e.g. H13 tools, under lubricated conditions could achieve similar results to using tools with a higher thermal conductivity, e.g. cast iron tools, under dry conditions. This feature would be beneficial to the reduction of the requirements of the forming press capabilities, as lower contact pressures could consequently be applied.

Theoretically, this model is also able to predict the effect of surface roughness on the IHTC evolutions. Fig. 11 shows the IHTC evolutions as a function of the surface roughness of the tool and specimen, predicted by the IHTC model, at a constant contact pressure of 15 MPa and thermal conductivities of 0.0244 and 0.14 kW/mK for the tool and specimen respectively, under dry conditions. In general, the IHTC

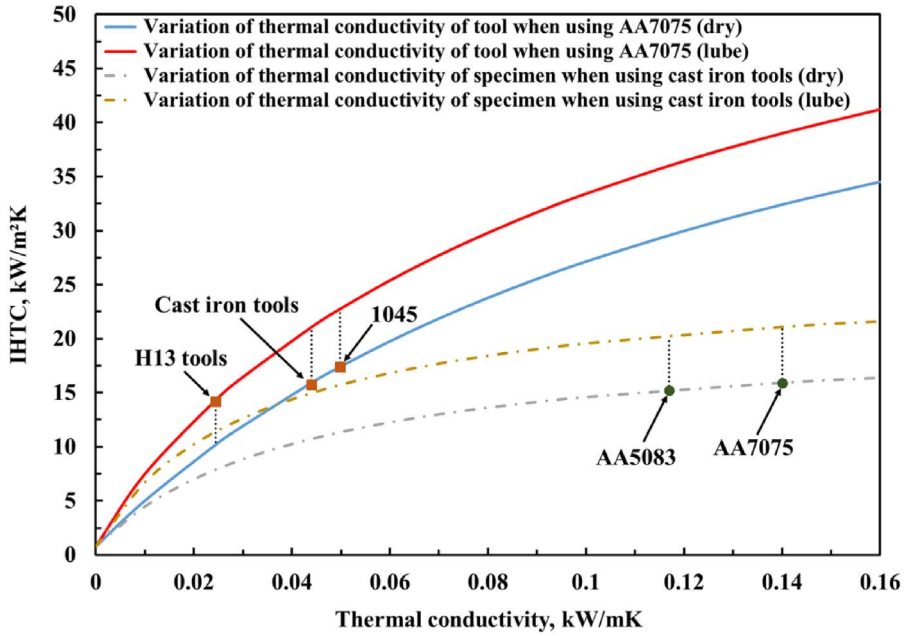

Fig. 10. The predicted IHTC evolutions as a function of the thermal conductivities of tool and specimen.

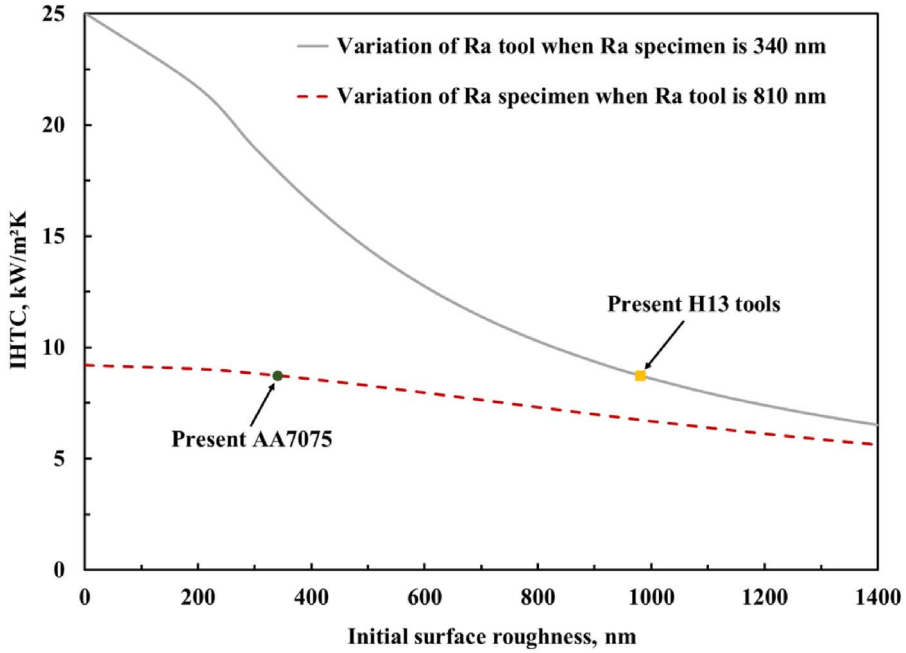

Fig. 11. The predicted IHTC evolutions as a function of the initial surface roughness of tool and specimen.

evolutions will decrease with the increasing surface roughness of the tool and specimen, due to the fact that the real contact area has an inverse relationship with the surface roughness. As discussed earlier, the surface roughness of the specimen approaches the value of that for the tools during a hot stamping process, due to the higher strength of the tools. The initial surface roughness of the tools before stamping is therefore crucial, whereas the value for the specimen has a marginal effect on the IHTC. The meshing between the two contact surfaces decreases with the increasing initial surface roughness of tools. Consequently, the real contact area and the IHTC values decrease. These predictions agree with the previous theoretical analysis.

5. Hot stamping validation tests

5.1. Experimental setup and procedures

Hemispherical dome and B pillar forming tests were conducted to measure the temperature evolutions of the blank during forming and validate the IHTC model by implementing it in simulations of the tests. The tool used for the hot stamping hemispherical dome forming tests is shown in Fig. 12, and comprises a hemispherical die with 100 mm diameter made from P20, a 180 × 180 × 2 mm^3 AA7075 blank, and a top and a bottom blankholder, whilst Fig. 13 shows the tool used for the B pillar tests, comprising a 310 × 200 × 2 mm^3 AA7075 blank, a blankholder, punch and a die, all made from P20.

In order to monitor the temperature for each test, a pair of thermocouples was embedded at a specific location of the blanks; at the middle of the blank for the hemispherical dome tests, and 110 mm away from the short edge and 10 mm away from the long edge of the blank for the B pillar tests, as shown in Figs. 14 and 15, and then connected to a thermometer. Prior to both the hemispherical and B pillar tests, the same grease-based graphite used in the IHTC model tests was applied as a lubricant with great care onto the tool surfaces, ensuring the lubricant layer thickness reached 0.015 mm to achieve the peak IHTC value. The blank was initially heated up to 490 °C and soaked for 3 min in a furnace. During the hemispherical dome test, the

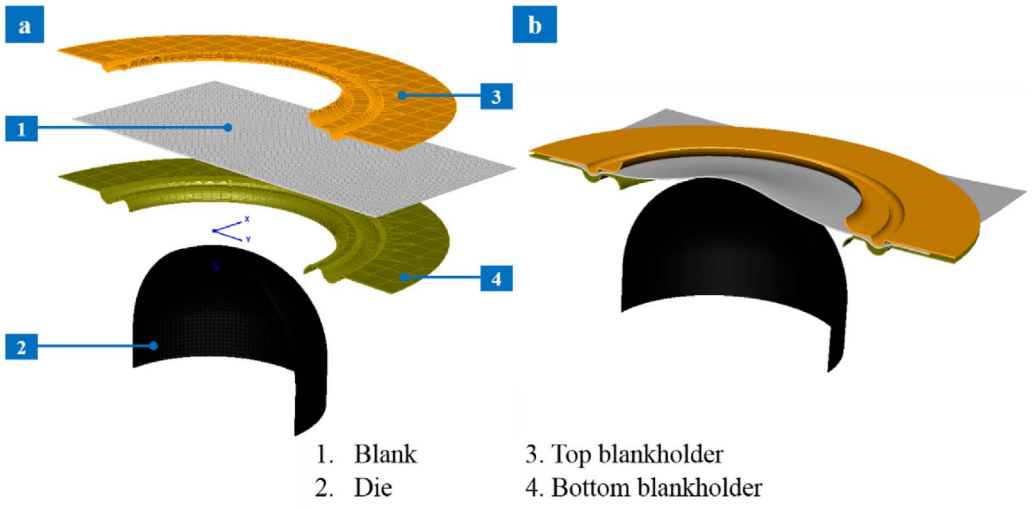

Fig. 12. The FE model of the hemispherical dome test in PAM-STAMP (cross-sectional view), under (a) the loading condition and (b) the forming condition.

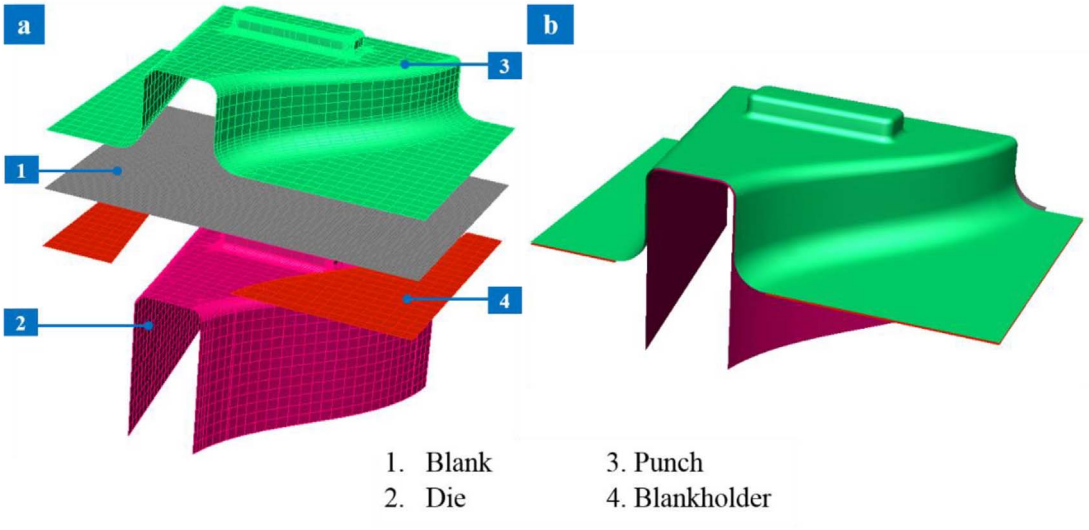

Fig. 13. The FE model of the B pillar test in PAM-STAMP under (a) the loading condition and (b) the forming condition.

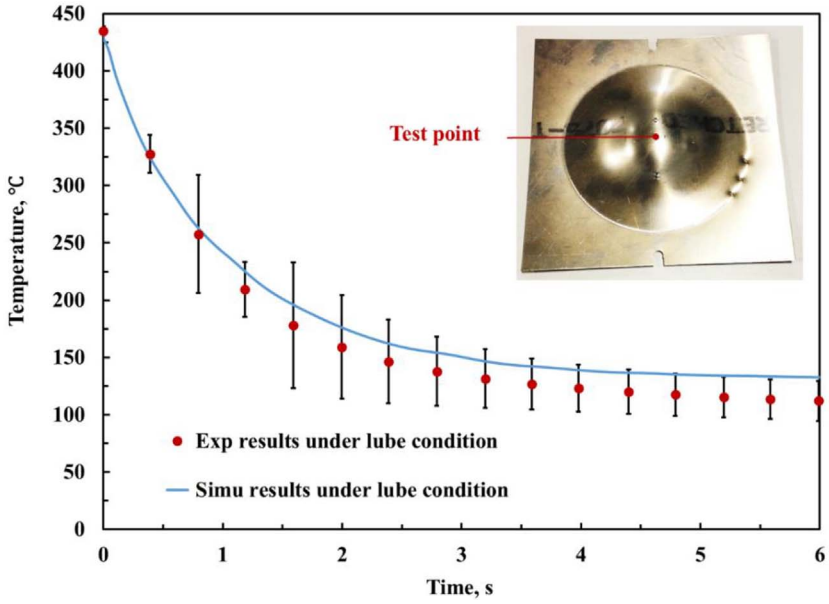

Fig. 14. The experimental and simulated temperature evolutions for the hemispherical dome tests under lubricated conditions.

hot blank was then transferred rapidly onto the bottom blankholder within 10 s. Once the blank temperature dropped to around 430 °C, the top blankholder was instantly actuated to move towards the blank and compress it against the bottom blankholder. The blankholding force was maintained by two gas springs at a constant value of 20 kn. The compressed blankholders continuously moved towards the cold static die at a speed of 75 mm/s to deform the blank to a dome height of 10 mm. After a 20 s quenching period, the top and bottom blankholders were returned to their initial positions. During the B pillar test, the hot blank was transferred quickly onto the blankholder after heating and soaking. When the temperature of the blank decreased to 430 °C, the punch was moved towards the static cold die immediately, compressing the blank against the blankholder at a constant blankholding force of 20 kn and subsequently deforming it into a B pillar shaped component at a stamping speed of 75 mm/s. The punch and the blankholder were then returned after a 20 s quenching stage.

5.2. FE simulation procedures for the validation tests

In order to simulate the hemispherical dome and B pillar forming tests, FE models for both were developed in PAM-STAMP. The dimensions of the blanks and tools were the same as those used in the experiments, as shown in Figs. 12 and 13. Explicit quadrangle thermal shell elements with a size of 2 mm were used for the blanks in both the hemispherical dome and B pillar FE simulations, which were identical to those used in the IHTC FE simulations. The initial temperature of the blank for both FE simulations was set as 430 °C, and the predicted IHTC evolutions with contact pressure using P20 tools and lubricated conditions were implemented in both FE simulations.

5.3. Validation results

As shown in Figs. 14 and 15, the simulated temperature evolutions were in close agreement with the experimental curves, indicating that the assigned IHTC evolutions and the IHTC model were validated by the hot stamping hemispherical dome and B pillar forming tests.

6. Conclusions

The interfacial heat transfer coefficient between hot blanks and cold

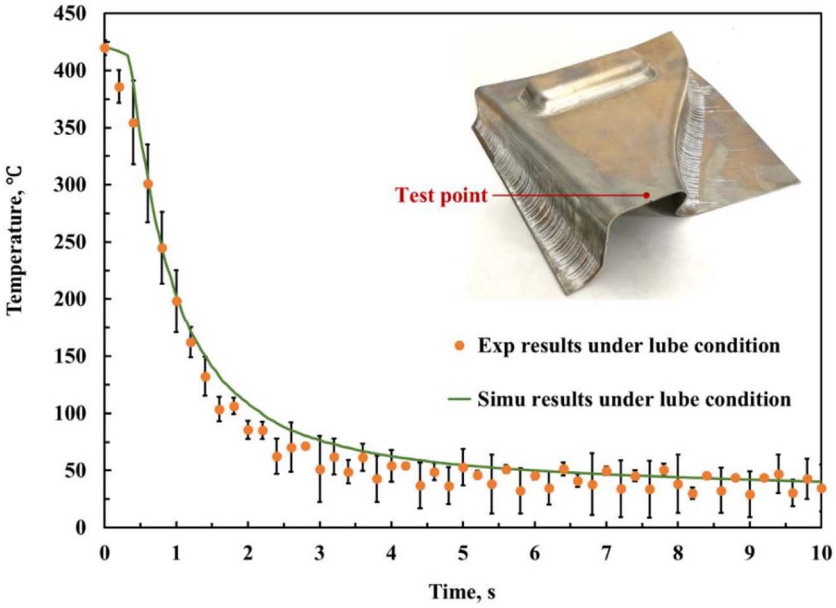

Fig. 15. The experimental and simulated temperature evolutions for the B pillar tests under lubricated conditions.

tools determines the quenching rate during hot stamping processes and whether the full mechanical strength of formed components can be retained. The IHTC values and critical quenching rates are critical for tool design. A novel experimental facility was designed to deduce the IHTC for any combination of blank and tool materials and contact pressure, under both dry and lubricated conditions. At the first instance, the IHTC test facility was used to measure temperature evolutions at a specific location on AA7075 blanks, which were then fit to simulated temperature evolutions obtained from the FE software PAM-STAMP, to investigate the effect of contact pressure on the IHTC using two different tool materials. A greased-based graphite lubricant was then applied onto the tool surfaces to research the effect of lubricant on the IHTC.

An exponential relationship between the IHTC and contact pressure was identified under both dry and lubricated conditions. Specifically, under dry conditions, the IHTC increases dramatically with increasing contact pressure and remains stable at 8.6 kW/m^2K at a contact pressure of 13 MPa using H13 tools. When cast iron tools were applied, the IHTC plateaus at 15.1 kW/m^2K after a contact pressure of 13 MPa was reached under dry conditions, whilst the IHTC peak value rises by 46%, to 22 kW/m^2K, when the grease-based graphite lubricant was applied at a layer thickness value of 0.015 mm. In addition, the IHTC was found to increase exponentially with the increasing applied lubricant layer thickness. When the layer thickness was larger than 0.015 mm, the IHTC remained constant at different contact pressures.

The IHTC model developed in the present research provides an effective approach for predicting IHTC evolutions as a function of contact pressure, tool materials and lubricant. The model was verified through further IHTC tests using P20 tools and validated through hot stamping hemispherical dome and B pillar forming tests. In future research, further IHTC experiments with different surface roughnesses for the specimens and tools will be performed in order to optimise the relationship between the IHTC and surface roughness in the model, and enhance the accuracy of the predictions.

Acknowledgements

Much appreciated is the strong support received from the CRRC Qingdao Sifang Co., Ltd (CRRC Sifang). The research was performed at the CRRC Sifang Centre for Rail Transportation Manufacturing Technologies at Imperial College London. This research was also supported by the China Scholarship Council (Grant CSC no. 201608060261): A non-profit institution enabling talented Chinese students to undertake a PhD programme overseas.

References

Çetinkale, T.N., Fishenden, M., 1951. Thermal conductance of metal surfaces in contact. In: Proceedings of International Conference of Heat Transfer. Institute of Mechanical Engineers. London UK. pp. 271–275.

Bai, Q., Lin, J., Zhan, L., Dean, T.A., Balint, D.S., Zhang, Z., 2012. An efficient closed-form method for determining interfacial heat transfer coefficient in metal forming. Int. J. Mach. Tools Manuf. 56, 102–110. http://dx.doi.org/10.1016/j.ijmachtools.2011.12.005.

Buchner, B., Buchner, M., Buchmayr, B., 2009. Determination of the real contact area for numerical simulation. Tribol. Int. 42, 897–901. http://dx.doi.org/10.1016/j.triboint.2008.12.009.

Burte, P.R., Im, Y., Altan, T., Semiatin, S.L., 1990. Measurement and analysis of heat transfer and friction during hot forging. J. Eng. Ind. 112, 332. http://dx.doi.org/10.1115/1.2899596.

Caron, E.J.F.R., Daun, K.J., Wells, M.A., 2014. Experimental heat transfer coefficient measurements during hot forming die quenching of boron steel at high temperatures. Int. J. Heat Mass Transf. 71, 396–404. http://dx.doi.org/10.1016/j.ijheatmasstransfer.2013.12.039.

Chang, Y., Tang, X., Zhao, K., Hu, P., Wu, Y., 2016. Investigation of the factors influencing the interfacial heat transfer coefficient in hot stamping. J. Mater. Process. Technol. 228, 25–33. http://dx.doi.org/10.1016/j.jmatprotec.2014.10.008.

Cooper, M.G., Mikic, B.B., Yovanovich, M.M., 1969. Thermal contact conductance. Int. J. Heat Mass Transf. 153, 317–323. http://dx.doi.org/10.1016/j.cbpa.2009.03.006.

Foster, A.D., Mohamed, M.S., Lin, J., Dean, T.A., Kensington, S., 2008. An investigation of lubricant and heat transfer for a sheet aluminium heat, form-quench (HFQ) process. Special Edition Metal Forming Conference.

Foster, A., Dean, T.A., Lin, J., 2013. Process for Forming Aluminium Alloy Sheet Components. (EP2324137B1).

Garrett, R.P., Lin, J., Dean, T.A., 2005. An investigation of the effects of solution heat treatment on mechanical properties for AA 6xxx alloys: experimentation and modelling. Int. J. Plast. 21, 1640–1657. http://dx.doi.org/10.1016/j.ijplas.2004.11.002.

Hu, Z.M., Brooks, J.W., Dean, T.A., 1998. The interfacial heat transfer coefficient in hot die forging of titanium alloy. Proc. Inst. Mech. Eng. Part C J. Mech. Eng. Sci. 212, 485–496. http://dx.doi.org/10.1243/0954406981521385.

Hu, P., Ying, L., Li, Y., Liao, Z., 2013. Effect of oxide scale on temperature-dependent interfacial heat transfer in hot stamping process. J. Mater. Process. Technol. 213, 1475–1483. http://dx.doi.org/10.1016/j.jmatprotec.2013.03.010.

Jain, V.K., 1990. Determination of heat transfer coefficient for forging applications. J. Mater. Shap. Technol. 8, 193–202. http://dx.doi.org/10.1007/BF02833814.

Ji, K., Fakir, O., El Gao, H., Wang, L., 2014. Determination of heat transfer coefficient for hot stamping process. In: Joint 3rd UK-China Steel Research Forum & 15th CMA-UK Conference on Materials Science and Engineering. Elsevier Ltd.. pp. 0–5. http://creativecommons.org/licenses/by-nc-nd/3.0/.

Johnson, B., 2004. Residual Stress Reduction During Quenching of Wrought 7075 Aluminum Alloy. Worchster Polytechnic Institute.

Karbasian, H., Tekkaya, A.E., 2010. A review on hot stamping. J. Mater. Process. Technol. 210, 2103–2118. http://dx.doi.org/10.1016/j.jmatprotec.2010.07.019.

Liu, X., Ji, K., Fakir, O., Liu, El, Zhang, J., Wang, Q., 2015. Determination of the interfacial heat transfer coefficient in the hot stamping of AA7075. 4th International Conference on New Forming Technology (ICNFT 2015). http://dx.doi.org/10.1051/matecconf/20152105003.

MatWeb, 2016. URL http://www.matweb.com/index.aspx.

Milkereit, B., Kessler, O., Schick, C., 2009. Recording of continuous cooling precipitation diagrams of aluminium alloys. Thermochim. Acta 492, 73–78. http://dx.doi.org/10.1016/j.tca.2009.01.027.

Shlykov, J.P., Ganin, E.A., Tsarevskiy, S., 1977. Thermal contact resistance. M Energy 328.

Wilson, W.R.D., Schmid, S.R., Liu, J., 2004. Advanced simulations for hot forging: heat transfer model for use with the finite element method. J. Mater. Process. Technol. 155–156, 1912–1917. http://dx.doi.org/10.1016/j.jmatprotec.2004.04.399.

Yukawa, N., Nakashima, Y., Ishiguro, T., Abe, E., Ishikawa, T., Choda, T., 2014. Modeling of heat transfer coefficient of oxide scale in hot forging. Procedia Eng. 81, 492–497. http://dx.doi.org/10.1016/j.proeng.2014.10.028.

Zhang, X.Z., Zhang, L.W., Xing, L., 2010. Study of thermal interfacial resistance between TC11/glass lubrication/K403 joint. Exp. Therm. Fluid Sci. 34, 48–52. http://dx.doi.org/10.1016/j.expthermflusci.2009.09.001.